How to cite: *Angew. Chem. Int. Ed.* **2021**, *60*, 17373–17377
International Edition: doi.org/10.1002/anie.202104955
German Edition: doi.org/10.1002/ange.202104955

Inorganic Chemistry

Liquid-Phase Synthesis of Highly Reactive Rare-Earth Metal Nanoparticles

*Daniel Bartenbach, Olivia Wenzel, Radian Popescu, Lara-Pauline Faden, Andreas Reiß, Michelle Kaiser, Anna Zimina, Jan-Dierk Grunwaldt, Dagmar Gerthsen, and Claus Feldmann**

Dedicated to Professor Hansgeorg Schnöckel on the occasion of his 80th birthday

Abstract: *The first liquid-phase synthesis of high-quality, small-sized rare-earth metal nanoparticles (1–3 nm)—ranging from lanthanum as one of the largest (187 pm) to scandium as the smallest (161 pm) rare-earth metal—is shown. Size, oxidation state, and reactivity of the nanoparticles are examined (e.g., electron microscopy, electron spectroscopy, X-ray absorption spectroscopy, selected reactions). Whereas the nanoparticles are highly reactive (e.g. in contact to air and water), they are chemically stable as THF suspensions and powders under inert conditions. The reactivity can be controlled to obtain inorganic and metal–organic compounds at room temperature.*

Rare-earth metals are highly reactive, in principle.[1] Performing reactions with rare-earth metals in a controlled manner is nevertheless difficult. On the one hand, the surface area of the bulk metals is small and crushing them into pieces is difficult due to their hardness and sensitivity. On the other hand, the surface of rare-earth metals is usually passivated by hydroxides, oxides, and/or carbonates, which kinetically inhibit reactions at low temperature. In chemical syntheses, these passivation layers naturally also cause impurities. However, a purification of rare-earth metals is elaborate and requires high-temperature distillation ($>800\,°C$), special equipment (e.g. steel cylinders), and profound experience.[2] In contrast to alkali metals and alkali earth metals, rare-earth metals also show only low solubility in liquid ammonia.[3] As a result, reactions with zerovalent rare-earth metals are often limited to high-temperature solid-state reactions ($>500\,°C$).[1,4]

The availability of rare-earth metals in the form of small-sized nanoparticles in suspension or as powder sample could significantly change the aforementioned situation and allow an easy handling with reactions of rare-earth metals near room temperature ($\leq 100\,°C$) and/or directly in the liquid phase. A liquid-phase synthesis of rare-earth metal nanoparticles, however, is largely unknown. This can be ascribed to the reactivity of such nanoparticles, which needs to be expected as considerably higher than for the respective bulk rare-earth metals. So far, few reports address physical methods to obtain rare-earth metal particles (e.g., γ-radiation, laser ablation, plasma treatment, electrodeposition),[5] which, however, result in heavily agglomerated particles with broad size distribution and significant oxygen contamination. Some reports claim aqueous syntheses or even biosyntheses,[6] which seems hardly traceable when considering the position of the rare-earth metals in the voltage series with electrochemical potentials of about −2.4 V.[7] Our experience is the observation of violent reactions with explosion if the rare-earth metal nanoparticles come into contact with water.

The dilemma of the high reactivity can be exemplarily illustrated for Gd^0 nanoparticles. Here, the only reliable liquid-phase synthesis relates to the reduction of $GdCl_3$ with crown-ether-stabilized alkalides (e.g. $[K(18\text{-crown-}6]^+[K]^-$) as powerful reducing agents.[8] Due to the high reactivity of the Gd^0 nanoparticles, the authors could only identify Gd_2O_3 nanoparticles via electron microscopy. Recently, they could validate the formation of Gd^0 for Gd@Au core–shell nanoparticles with a dense gold shell to protect the Gd^0 core from oxidation.[8a] With La^0, Ce^0, Sm^0, Eu^0, Tm^0, Y^0, and Sc^0, we now present a reliable liquid-phase synthesis of high-quality, small-sized rare-earth metal nanoparticles ranging from lanthanum as a large (187 pm) to scandium as the smallest (161 pm) rare-earth metal for the first time (Figure 1a).[9]

Several prerequisites need to be addressed to obtain high-quality nanoparticles of such highly reactive metals. This includes a powerful reducing agent as well as a sample

[*] Dr. D. Bartenbach, M. Sc. L.-P. Faden, M. Sc. A. Reiß, M. Sc. M. Kaiser, Prof. Dr. C. Feldmann
Institute for Inorganic Chemistry, Karlsruhe Institute of Technology (KIT)
Engesserstraße 15, 76131 Karlsruhe (Germany)
E-mail: claus.feldmann@kit.edu
Dr. O. Wenzel, Dr. R. Popescu, Prof. Dr. D. Gerthsen
Laboratory for Electron Microscopy, Karlsruhe Institute of Technology (KIT)
Engesserstrasse 7, 76131 Karlsruhe (Germany)
Dr. A. Zimina, Prof. Dr. J.-D. Grunwaldt
Institute of Catalysis Research and Technology, Karlsruhe Institute of Technology (KIT)
Hermann-von-Helmholtz-Platz 1, 76344 Eggenstein-Leopoldshafen (Germany)
Prof. Dr. J.-D. Grunwaldt
Institute for Chemical Technology and Polymer Chemistry, Karlsruhe Institute of Technology (KIT)
Engesserstraße 20, 76131 Karlsruhe (Germany)
Supporting information and the ORCID identification number(s) for the author(s) of this article can be found under: https://doi.org/10.1002/anie.202104955.

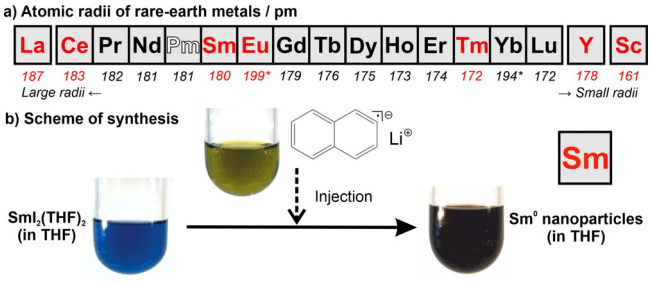

Figure 1. Rare-earth metals: a) Row of metals with atomic radii (red-marked metals prepared here, *aperiodic radii due to half-filled f^7 and filled f^{14} electron shell). b) Scheme of the exemplary liquid-phase synthesis of Sm^0 nanoparticles.

handling under strict inert conditions, starting from synthesis to all analytical characterization. Based on our experience with base metal nanoparticles (e.g., Ti^0, Mo^0, W^0, Re^0, Fe^0, Zn^0) and different synthesis strategies (e.g., microemulsions with liquid ammonia, sodium-driven reduction in liquid ammonia, lithium/sodium naphthalenide-driven reduction in tetrahydrofuran, lithium/sodium pyridinyl-driven reduction in pyridine),[10] we have selected lithium naphthalenide ([LiNaph]) as the reducing agent of choice to obtain the even more reactive rare-earth metals. Simple metal halides were used as low-cost, well-soluble starting materials (see SI). All syntheses were performed in Schlenk-type vessels; sample handling and centrifugation were carried out in gloveboxes; suitable transfer systems were used for all analytical characterization (SI: Figure S1).

The synthesis strategy is exemplarily illustrated for Sm^0 nanoparticles (Figure 1b). Accordingly, $SmI_2(THF)_2$ was dissolved in tetrahydrofuran (THF). Moreover, lithium and naphthalene were dissolved in THF. Thereafter, the resulting [LiNaph] solution was injected with intense stirring into the $SmI_2(THF)_2$ solution. The reduction and nucleation of Sm^0 nanoparticles are indicated by the immediate formation of a deep black suspension after injection of [LiNaph]. Electron paramagnetic resonance (EPR) spectra confirm the completeness of the reaction (SI: Table S1, Figure S2). Thus, the ESR signal of the paramagnetic [LiNaph] vanishes completely upon reduction of $SmI_2(THF)_2$. Subsequent to the reaction, the Sm^0 nanoparticles were separated by high-power centrifugation (25.000 rpm, 55.200 × g), purified by resuspension/centrifugation in/from THF or toluene. The as-prepared nanoparticles can be easily redispersed in THF or toluene, or they can be dried in vacuum at room temperature to obtain powder samples.

Size, shape, and size distribution of the as-prepared Sm^0 nanoparticles were evaluated by transmission electron microscopy (TEM) (Figure 2). Overview TEM images show uniform, non-agglomerated nanoparticles with narrow size distribution (Figure 2a,b). A statistical evaluation of 250 nanoparticles on TEM images results in a mean diameter of 1.7 ± 0.2 nm (Figure 2c). High-resolution (HR)TEM images confirm a size of 1–3 nm (Figure 2d). Moreover, HRTEM indicates the crystallinity of the as-prepared Sm^0 nanoparticles and shows highly parallel lattice fringes (Figure 2d). The observed lattice fringe distance of 1.9 Å is well compatibel

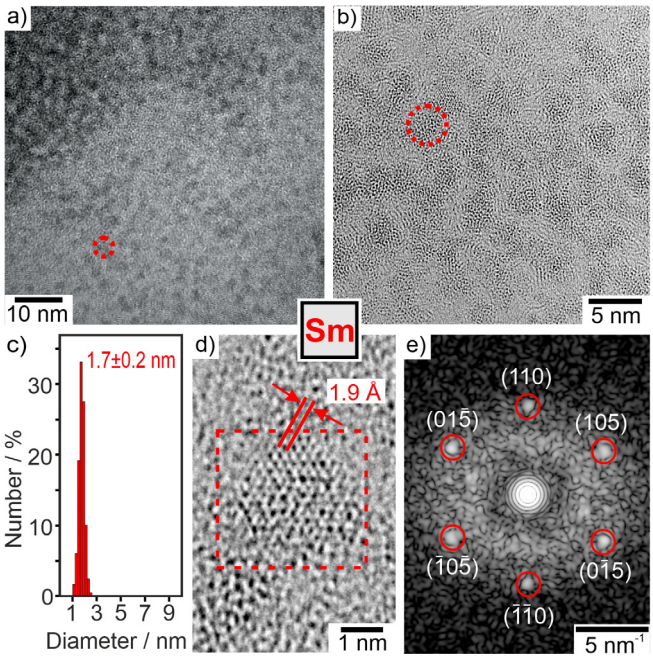

Figure 2. Electron microscopy of the as-prepared Sm^0 with a,b) TEM images at different levels of magnification (red dots indicate single nanoparticles), c) size distribution (based on statistical evaluation of 250 nanoparticles on TEM images), d) HRTEM image with lattice fringes, e) FT-HRTEM image in (c) with reflection positions of calculated diffraction pattern in [-551] zone axis indicated by red circles.

with hexagonal β-Sm^0 (d_{105} with 1.9 Å).[11] The presence of zerovalent Sm is further confirmed by Fourier transformation (FT) analysis of HRTEM images of single particles (Figure 2e), which agrees with the calculated diffraction pattern of hexagonal bulk-Sm^0 (space group: $P6_3/mmc$, $a = 3.682$, $c = 11.043$ Å) in the [-551] zone axis.[11] We also observed few particles with disordered structure (Figure 2b), which could be caused by electron-beam-induced knock-on damage. The formation of very small Sm^0 nanoparticles might be surprising at first sight, but is well in agreement with the LaMer-Dinegar model of particle nucleation and growth.[12] Thus, the injection of [LiNaph] initiates a fast reduction and formation of metal nanoparticles, which are highly insoluble in THF. The resulting high oversaturation promotes a fast nucleation and, therefore, very small particles.

In addition to HRTEM and FFT analysis, the oxidation state of the as-prepared Sm^0 nanoparticles was validated by X-ray absorption near edge structure (XANES) spectroscopy, electron energy loss spectroscopy (EELS), and energy-dispersive X-ray spectroscopy (EDXS). Sm-XANES L_3-edge spectra of the as-prepared nanoparticles were compared to bulk samarium, $SmI_2(THF)_2$, and literature data of Sm^0 clusters isolated in argon matrices (Figure 3, SI: Figure S3,S4). Particularly striking is the high intensity pre-edge peak of $SmI_2(THF)_2$ in the L_3-edge spectra, which can be ascribed to a $2p^6 \ldots 4f^6\ 6s^0 \rightarrow 2p^5 \ldots 4f^7\ 6s^0$ transition on Sm^{+II} (Figure 3a). This pre-edge peak is totally missing for the nanoparticles. In comparison to bulk Sm^0, however, the Sm^0 nanoparticles exhibit a double-peak structure (6708, 6716 eV). This double-peak structure was similarly reported

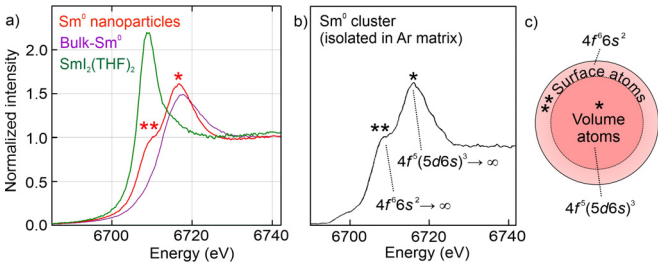

Figure 3. XANES spectra of the as-prepared Sm^0 nanoparticles: a) Sm-L_3 spectra with bulk metal and $SmI_2(THF)_2$ as references. b) Comparison with Ar-matrix-isolated Sm clusters.[13a] c) Scheme of Sm^0 nanoparticle with different electron configuration of volume atoms (indicated by *) and surface atoms (indicated by **) according to literature data.[13]

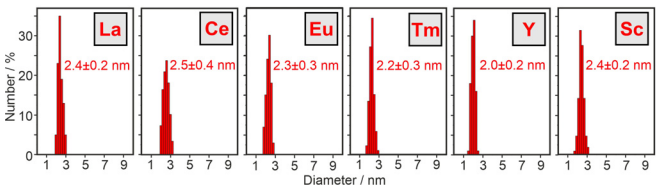

Figure 5. Size distribution of the as-prepared La^0, Ce^0, Eu^0, Tm^0, Y^0, and Sc^0 nanoparticles (statistical evaluation of 250 nanoparticles on TEM images).

for Ar-matrix-isolated samarium clusters and ascribed to a different valence electron configuration of volume and surface Sm atoms (Figure 3b).[13] Thus, Sm atoms in the cluster volume exhibit a $4f^5(5d\ 6s)^3$ configuration, whereas Sm atoms located at the cluster surface have a $4f^6\ 6s^2$ configuration with a shift of 8 eV between the two peaks (Figure 3a,b).[13] The intensity of both peaks depends on the size of the cluster. For the as-prepared Sm^0 nanoparticles with an average size of 1.7 ± 0.2 nm about 40 % of the Sm atoms are located at the surface, so that a significant contribution of surface atoms in the XANES spectra is not a surprise. Taken together, XANES spectra prove the presence of small-sized, zerovalent Sm nanoparticles, which was also confirmed by EELS and EDXS (SI: Figure S5,S6).

Similar to Sm^0, size, size distribution, and crystallinity of the as-prepared La^0, Ce^0, Eu^0, Tm^0, Y^0, and Sc^0 nanoparticles were also examined by TEM (Figure 4, SI: Figure S7–S12). Overview TEM images again show uniform, non-agglomerated nanoparticles with predominantly spherical shape (Figure 4a–f) and mean diameters of 2–3 nm at very narrow size distribution (± 0.3 nm) (Figure 5). HRTEM images prove the crystallinity of the as-prepared nanoparticles and show highly parallel lattice fringes (Figure 4a–f). The observed lattice fringe distances are well compatible with bulk metals (La^0: $d_{01\text{-}1}$ with 3.265 Å, Ce^0: $d_{1\text{-}1\text{-}1}$ with 3.071 Å, Eu^0: d_{002} with 2.695 Å, Tm^0: $d_{11\text{-}1}$ with 2.693 Å, Y^0: $d_{1\text{-}1\text{-}1}$ with 2.785 Å, Sc^0: $d_{1\text{-}1\text{-}1}$ with 2.51 Å).[14] Crystallinity and crystal structure of the as-prepared rare-earth metal nanoparticles were also confirmed by FT analysis (SI: Figure S7–S12). The crystallographic data are not only consistent with the bulk metals, they also differ clearly from the corresponding metal oxides (SI: Table S2).

With La^0 as a large and Sc^0 as the smallest rare-earth metal, the synthesis strategy is suitable to obtain all rare-earth metals as nanoparticles in the liquid phase. Having high-quality nanoparticles as a new form of rare-earth metals available for the first time, we also got a first glimpse on their reactivity and their use as starting materials in chemical synthesis. Under inert conditions (argon, nitrogen, vacuum), the as-prepared suspensions (THF, toluene) and powder samples are chemically very stable. Attention must be paid if the nanoparticles get into contact with oxidizing agents. Again, we take the Sm^0 nanoparticles as example. Here, direct contact of a powder sample (≈ 20 mg) to air causes an immediate reaction with sting flame (Figure 6a).

Beside the uncontrolled reaction of the as-prepared Sm^0 powders in air, we have exemplarily reacted the Sm^0 nanoparticles with NH_3, N_2H_4, S_8, I_2, ethanol (EtOH), and cyclopentadiene (HCp) at room temperature (25 °C) in the liquid phase (Figure 6b, SI: Figure S13–S26). The respective reactions are already indicated by the change of the deep black Sm^0 suspension to colorless, yellowish or red solutions/suspensions and result in different inorganic and metal-organic ocmpounds, including $Sm(NH_2)_3(THF)$, $Sm(N_2H_3)_3$-

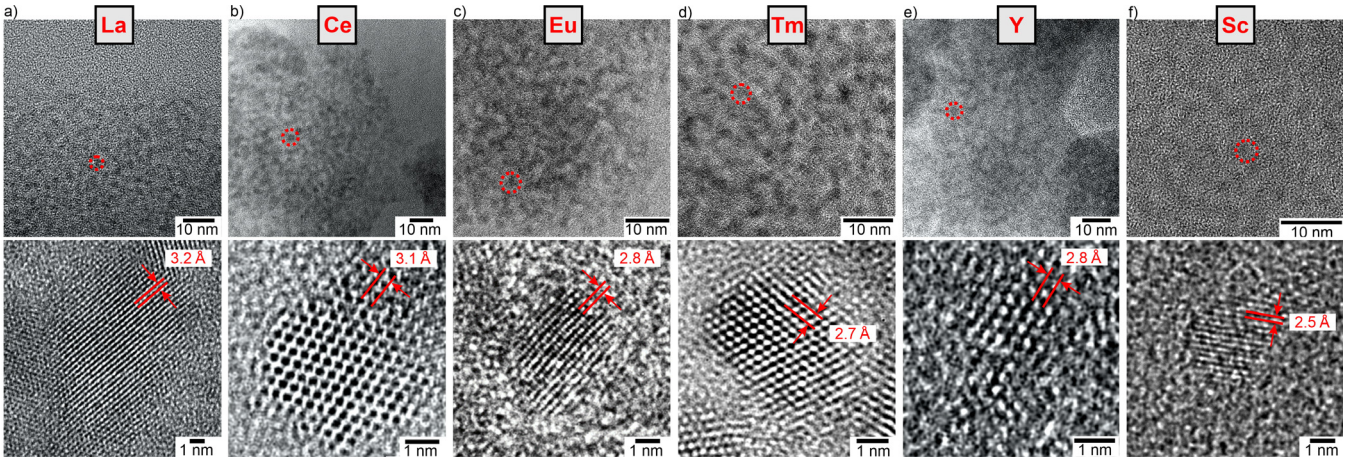

Figure 4. Electron microscopy of the as-prepared La^0, Ce^0, Eu^0, Tm^0, Y^0, Sc^0 with overview TEM images (red dots indicate single nanoparticles) and HRTEM images with lattice fringes, see SI for more data: Figure S7–S12).

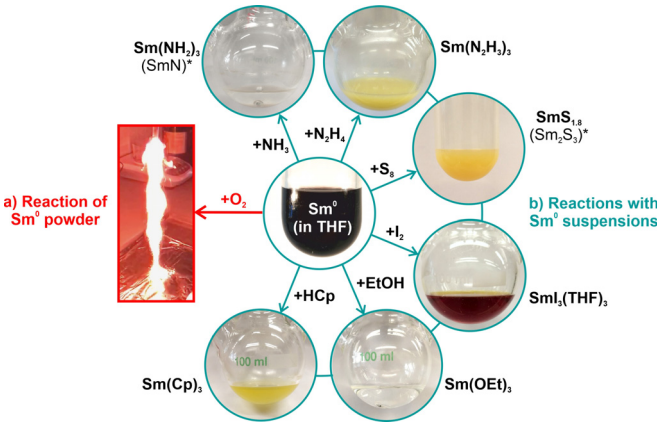

Figure 6. Reactivity of the as-prepared Sm^0 nanoparticles: a) uncontrolled, violent reaction in air (20 mg Sm^0 powder), b) controlled reactions with NH_3, N_2H_4, S_8, I_2, EtOH, HCp at 25 °C in the liquid phase (Sm^0 suspensions in THF).

(THF), $SmS_{1.8}$, $SmI_3(THF)_3$, $Sm(OEt)_3$, and $Sm(Cp)_3$ (SI: Figure S14–S26). After separation from the liquid-phase, $Sm(NH_2)_3(THF)$ and $SmS_{1.8}$ can be thermally converted to SmN and Sm_2S_3 (SI: Figure S15,S16,S19,S20). Depending on the respective reaction and compound, nanoparticles ($SmS_{1.8}$, SI: Figure S18) or even single crystals ($SmI_3(THF)_3$, $Sm(Cp)_3$, SI: Table S3, Figure S21,S22,S25) can be obtained. Moreover, $Sm(N_2H_3)_3(THF)$ and $SmI_3(THF)_3$ are already new compounds (SI: Figure S17,S22). The reaction of the Sm^0 nanoparticles with N_2H_4 resulted in an unusual metal hydrazide, which is even more reactive than the intial Sm^0 (see SI). Such reaction was yet only reported for alkali metals[15] and points to the reactivity of the rare-earth metal nanoparticles. Even more interesting than each of the aforementioned follow-up reactions, however, might be the general option to use the as-prepared rare-earth metal nanoparticles in a controlled manner as starting materials in chemical syntheses near room temperature (≤ 100 °C) and/or instantaneously in the liquid phase.

For all kinds of liquid-phase syntheses, it is a matter of course that the as-prepared nanoparticles contain at least the solvent as surface capping. In this regard, FT-IR spectra show THF to be adsorbed on the surface of the as-prepared nanoparticles (SI: Figure S13). Taking the high reactivity of the rare-earth metal nanoparticles into account, however, it is a surprise as such that the nanoparticles are chemically stable in suspension. Moreover, a small-sized, low-weight molecule like THF as the surface capping is beneficial for follow-up reactions as it can be easily exchanged by other, stronger-binding ligands, which then can be chosen independent from the original nanoparticle synthesis. Our exemplary reactions already indicate products that do not contain THF (e.g., $SmS_{1.8}$, $Sm(OEt)_3$, $Sm(Cp)_3$).

In sum, a reliable liquid-phase synthesis of rare-earth metal nanoparticles is shown for the first time with La^0, Ce^0, Sm^0, Eu^0, Tm^0, Y^0, and Sc^0 as examples. The synthesis uses metal halides as low-cost starting materials, THF as conventional solvent, and [LiNaph] as a powerful, easy-to-handle reducing agent. The as-prepared rare-earth metal nanoparticles exhibit very small sizes (1–3 nm) and narrow size distributions (± 0.3 nm). They are monocrystalline and well-dispersible in THF or toluene. Whereas the rare-earth metal nanoparticles are chemically stable under inert conditions, they show heavy reactivity, for instance, in contact to air. However, the reactivity can be well-controlled, so that the rare-earth metal nanoparticles can be exemplarily reacted with NH_3, N_2H_4, S_8, I_2, EtOH and HCp to obtain different inorganic and metal-organic compounds at room temperature and instantaneously in the liquid phase. Having the first liquid-phase synthesis of rare-earth metal nanoparticles established, these nanoparticles might become most interesting as starting materials to prepare new and/or high-purity rare-earth metal compounds as well as rare-earth-metal-based materials.

Acknowledgements

C.F. and D.G. are grateful to the Deutsche Forschungsgemeinschaft (DFG) for funding of personnel (FE911/11-1, GE 841/29-1: *"NanoMet"*) and TEM equipment (INST 121384/33-1 FUGG). C.F. and J.D.G. also acknowledge the DFG Collaborative Research Centre on catalysis (CRC1441: *"TrackAct"*). Open access funding enabled and organized by Projekt DEAL.

Conflict of interest

The authors declare no conflict of interest.

Keywords: follow-up reactions · liquid-phase synthesis · nanoparticles · rare-earth metals

[1] D. A. Atwood, *The Rare Earth Elements: Fundamentals and Applications*, Wiley-VCH, Weinheim, **2012**.
[2] G. Brauer, *Handbuch der präparativen Anorganischen Chemie*, *Vol. 2*, Enke, Stuttgart, **1978**, pp. 1071.
[3] a) C. C. Quitmann, K. Mueller-Buschbaum, *Angew. Chem. Int. Ed.* **2004**, *43*, 5994; *Angew. Chem.* **2004**, *116*, 6120; b) E. O. Fischer, H. Fischer, *Angew. Chem. Int. Ed. Engl.* **1964**, *3*, 132; *Angew. Chem.* **1964**, *76*, 52.
[4] a) F. G. N. Cloke, *Chem. Soc. Rev.* **1993**, *22*, 17; b) A. Simon, *Pure Appl. Chem.* **1995**, *67*, 311.
[5] a) A. Urumese, R. N. Jenjeti, S. Sampath, B. R. Jagirda, *J. Colloid Interface Sci.* **2016**, *476*, 177; b) V. I. Petinov, *Russ. J. Phys. Chem. A* **2016**, *90*, 1413; c) Q. Xu, S. Hu, W. Wang, Y. Wang, H. Ju, X. Zhu, *Appl. Surf. Sci. B* **2018**, *432*, 115; d) Y. N. Ertas, N. N. Jarenwattananon, L.-S. Bouchard, *Chem. Mater.* **2015**, *27*, 5371; e) S. Chall, A. Saha, S. K. Biswas, A. Datta, S. C. Bhattacharya, *J. Mater. Chem.* **2012**, *22*, 12538; f) N. V. Tarasenko, A. V. Buthsen, A. A. Nevar, *Appl. Phys. A* **2008**, *93*, 837; g) I. Aruna, B. R. Metha, L. K. Malhotra, S. M. Shivaprasad, *Adv. Funct. Mater.* **2005**, *15*, 131; h) Z. C. Yan, Y. H. Huang, Y. Zhang, H. Okumara, J. Q. Xiao, S. Stoyanov, V. Skumryev, G. C. Hadjipanayis, *Phys. Rev. B* **2003**, *67*, 054403.
[6] a) K. A. Manoj Kumar, E. Hemananthan, P. R. Devi, S. V. Kumar, R. Hariharan, *Mater. Today* **2017**, *21*, 887; b) A. Chatterjee, L. Archana, V. Niroshinee, J. Abraham, *Res. J. Pharmaceut. Biol. Chem. Sci.* **2016**, *7*, 1462; c) V. Sankar, P. SalinRaj, R. Athira, R. Sreenivasan Soumya, K. Gopalan Ra-

ghu, *RSC Adv.* **2015**, *5*, 21074; d) J. A. Ascencio, A. C. Rincon, G. Canizal, *J. Phys. Chem. B* **2005**, *109*, 8806.
[7] A. F. Holleman, E. Wiberg, *Anorganische Chemie*, *Vol. 1*, 103. ed., de Gruyter, Berlin, **2017** Annex III/IV.
[8] a) C. Yan, M. J. Wagner, *Nano Lett.* **2013**, *13*, 2611; b) J. A. Nelson, L. H. Bennet, J. J. Wagner, *J. Am. Chem. Soc.* **2002**, *124*, 2979.
[9] http://www.webelements.com (scandium and lanthanum).
[10] a) C. Schöttle, P. Bockstaller, D. Gerthsen, C. Feldmann, *Chem. Commun.* **2014**, *50*, 4547; b) F. Gyger, P. Bockstaller, D. Gerthsen, C. Feldmann, *Angew. Chem. Int. Ed.* **2013**, *52*, 12443; *Angew. Chem.* **2013**, *125*, 12671; c) C. Schöttle, P. Bockstaller, R. Popescu, D. Gerthsen, C. Feldmann, *Angew. Chem. Int. Ed.* **2015**, *54*, 9866; *Angew. Chem.* **2015**, *127*, 10004; d) A. Egeberg, T. Block, O. Janka, O. Wenzel, D. Gerthsen, R. Pöttgen, C. Feldmann, *Small* **2019**, *15*, 1902321.
[11] N. L. Shi, D. Fort, *J. Less-Common Met.* **1985**, *113*, 21.
[12] V. K. LaMer, R. H. J. Dinegar, *J. Am. Chem. Soc.* **1950**, *72*, 4847.
[13] a) M. Lübcke, B. Sonntag, W. Niemann, P. Rabe, *Phys. Rev. B* **1986**, *34*, 5184; b) M. G. Mason, S. T. Lee, G. Apai, R. F. Davies, D. A. Shirley, A. Franciosi, J. A. Weaver, *Phys. Rev. Lett.* **1981**, *47*, 730.
[14] a) F. H. Spedding, J. J. Hanak, A. H. Daane, *J. Less-Common Met.* **1961**, *3*, 110; b) K. A. Gschneidner, R. O. Elliott, R. R. McDonald, *J. Phys. Chem. Solids* **1962**, *23*, 555; c) R. O. Demchyna, S. I. Chykhrij, Y. B. Kuz'ma, *J. Alloys Compd.* **2002**, *345*, 170; d) B. Hájek, V. Brožek, P. H. Duvigneaud, *J. Less-Common Met.* **1973**, *33*, 385.
[15] J. Goubeau, U. Kull, *Z. Anorg. Allg. Chem.* **1962**, *316*, 182.
[16] W. J. Evans, T. S. Gummersheimer, J. W. Ziller, *J. Am. Chem. Soc.* **1995**, *117*, 8999.

Manuscript received: April 11, 2021
Accepted manuscript online: April 30, 2021
Version of record online: June 29, 2021

